

Provided for non-commercial research and education use.  
Not for reproduction, distribution or commercial use.



Volume 265, Issues 3–4

30 January 2008

ISSN 0012-821X

# EARTH & PLANETARY SCIENCE LETTERS



This article was published in an Elsevier journal. The attached copy is furnished to the author for non-commercial research and education use, including for instruction at the author's institution, sharing with colleagues and providing to institution administration.

Other uses, including reproduction and distribution, or selling or licensing copies, or posting to personal, institutional or third party websites are prohibited.

In most cases authors are permitted to post their version of the article (e.g. in Word or Tex form) to their personal website or institutional repository. Authors requiring further information regarding Elsevier's archiving and manuscript policies are encouraged to visit:

<http://www.elsevier.com/copyright>



ELSEVIER

Available online at [www.sciencedirect.com](http://www.sciencedirect.com)

Earth and Planetary Science Letters 265 (2008) 641–654

EPSL

[www.elsevier.com/locate/epsl](http://www.elsevier.com/locate/epsl)

# Static compression of hydrous silicate melt and the effect of water on planetary differentiation

Carl B. Agee

*Institute of Meteoritics, Department of Earth and Planetary Sciences, University of New Mexico, Albuquerque, NM 87131, USA*

Received 25 July 2007; received in revised form 26 October 2007; accepted 4 November 2007

Available online 17 November 2007

Editor: G.D. Price

## Abstract

High pressure experiments using the sink/float method have bracketed the density of hydrous iron-rich ultrabasic silicate melt from 1.35 to 10.0 GPa at temperatures from 1400 to 1860 °C. The silicate melt composition was a 50–50 mixture of natural komatiite and synthetic fayalite. Water was added in the form of brucite  $\text{Mg}(\text{OH})_2$  and was present in the experimental run products at 2 wt.% and 5 wt.% levels as confirmed by microprobe analyses of total oxygen. Buoyancy marker spheres were olivines and garnets of known composition and density. The density of the silicate melt with 5 wt.% water at 2 GPa and 1500 °C is  $0.192 \text{ g cm}^{-3}$  less than the anhydrous form of this melt at the same  $P$  and  $T$ . This density difference gives a partial molar volume of water in silicate melt of  $\sim 7 \text{ cm}^3 \text{ mol}^{-1}$ , which is similar to previous studies at high pressure. The komatiite–fayalite liquids with 0 and 2 wt.%  $\text{H}_2\text{O}$ , have extrapolated density crossovers with equilibrium liquidus olivine at 8 and 9 GPa respectively, but there is no crossover for the liquid with 5 wt.%  $\text{H}_2\text{O}$ . These results are consistent with the hypothesis that dense hydrous melts could be gravitationally stable atop the 410 km discontinuity in the Earth. The results also support the notion that equilibrium liquidus olivine could float in an FeO-rich hydrous martian magma ocean. Extrapolation of the data suggests that FeO-rich hydrous melt could be negatively buoyant in the Earth's  $D''$ -region or atop the core–mantle–boundary (CMB), although experiments at higher pressure are needed to confirm this prediction.

© 2007 Elsevier B.V. All rights reserved.

**Keywords:** hydrous silicate melt; liquid compressibility; water; high pressure experiments; differentiation; olivine flotation; Mars; lower mantle; magma ocean

## 1. Introduction

Knowledge of the properties of melts at high pressure is of primary importance for understanding differentiation and dynamics in the Earth's interior. For the early Earth, melting greatly influenced crust, mantle and core formation. Indeed, estimates of energy release from

accretion and/or a Moon-forming giant impact predict wholesale melting of the proto-Earth, the impactor, and the debris that formed the Moon (Cameron and Benz, 1991). Recent results from Hf–W isotope chronometry (Yin et al., 2002; Kleine et al., 2002) argue for rapid planetary accretion and a core formation timescale that is also consistent with a hot early Earth. Siderophile element partitioning experiments point to a mantle–core equilibration at high pressure in a deep magma ocean in

*E-mail address:* [agee@unm.edu](mailto:agee@unm.edu).

the primordial Earth (Li and Agee, 1996; Chabot et al., 2005). In such very high-temperature environments, densities of melts and coexisting crystals as well as percolative fluid flow govern liquid/solid segregation and control to a significant extent the nature of the early Earth's internal structure (Ohtani, 1985; Agee and Walker, 1988a; Agee, 1998; Ohtani, 1984; Miller et al., 1991b). Over the past 20 yr there have been a number of experimental and theoretical studies which predict that anhydrous basic and ultrabasic silicate melts become denser than coexisting crystalline phases in both the Earth's upper and lower mantles (Agee, 1998; Rigden et al., 1984; Rigden et al., 1988; Agee and Walker, 1993; Suzuki et al., 1995; Ohtani, 1987, 1983; Stolper et al., 1981; Ohtani and Maeda, 2001; Agee and Walker, 1988b; Miller et al., 1991a) as well as the mantles of the Moon and Mars (Circone and Agee, 1996; Smith and Agee, 1997; Ohtani et al., 1995; Delano, 1990). Crystal–liquid density inversions (also called “cross-overs”) may have profound effects on planetary differentiation in the presence of deep mantle melting or a magma ocean (Ohtani, 1985; Agee and Walker, 1988a; Miller et al., 1991a; Nisbet and Walker, 1982; Morse, 1993; Solomatov and Stevenson, 1993).

There is a growing realization that mantle melting, both primordial and recent, may frequently involve significant participation of volatiles, especially water. For example, it has been proposed that a dense, blanketing, water-rich atmosphere will exchange nontrivial amounts of H<sub>2</sub>O with an early magma ocean (Abe et al., 2000). Numerous experiments have shown that the stability of several hydrous phases at high pressure make it possible to sequester subducted H<sub>2</sub>O at least as deep as the upper mantle transition zone and perhaps to the base of the lower mantle [see review in (Abe et al., 2000)]. Hydrated mantle will have solidus temperatures much lower than dry mantle rock (Green, 1973), thus partial melting in the deep mantle may be more likely to feature hydrous silicate liquids. The idea of hydrous melts residing in the upper mantle is supported by seismic studies that observe anomalously low S-wave velocities in some parts of the transition zone and have been interpreted to be caused by small degrees of hydrous melt trapped by neutral buoyancy in a rock matrix (Nolet and Zielhuis, 1994; Revenaugh and Sipkin, 1994). Bercovici and Karato (2003) hypothesized that dense hydrous melts in the upper mantle transition zone could retain incompatible elements thus explaining some of the geochemical differences between ocean–island and mid-ocean-ridge basalts. Ohtani et al. (2004) proposed that the mantle is layered with respect to water storage potential, with the transition zone having the highest water retention capacity. They

speculated that the pressure effect on partial molar volume of water at high pressure could allow hydrous melts (1 wt.% H<sub>2</sub>O) to exceed the density of crystalline phases in the transition zone. The D'' layer at the base of the lower mantle is also a region that may contain dense, negatively buoyant hydrous melts (Williams and Garnero, 1998). The source of volatiles could be from subducted slabs or from exsolution from outer core crystallization. Ohtani and Maeda (2001) propose that increasing the volatile content of these melts may cause density decreases sufficient to initiate gravitational instabilities contributing to plume formation and the generation of kimberlites.

Crystal–liquid density crossovers are not unique to the Earth. Earlier studies have demonstrated that liquidus olivine and pyroxene flotation can exist in the mantle of the Earth's Moon (Circone and Agee, 1996; Smith and Agee, 1997; Delano, 1990). Ohtani et al. (1995) were among the first to propose that the early martian mantle might be subject to crystal–liquid density crossovers. Recent work (McSween et al., 2001) indicates that some shergottite parent melts may have had up to 2% H<sub>2</sub>O, and this level of water concentration may have a significant effect on the density and compressibility of martian magmas, and on the depth of crystal–liquid density crossovers in an early, hydrous martian magma ocean. Indeed, an early Mars accreted from hydrated planetesimals could have had even higher levels of water incorporated in its mantle (see for example (Solomon et al., 2005)).

Until recently experimental data on the density and compressibility of hydrous silicate liquids was quite limited both in terms of pressure and composition. Pioneering work by Burnham and Davis (1971) determined the volume of hydrous albite melts up to 0.85 GPa. These data were the first published direct measurements of a silicate liquid at high pressure. Ochs and Lange, (1997, 1999) measured the densities of hydrous albite, KCS, and rhyolite glasses at 1-bar up to the glass transition temperatures and combined them with the Burnham and Davis data, and with volume data on anhydrous liquids (e.g. (Lange and Carmichael, 1987)), to allow calculation of hydrous silicate liquid densities at crustal magmatic conditions. The Ochs and Lange (O&L) data and calculations suggest that H<sub>2</sub>O will increase both the 1 bar compressibility and molar volume of mantle melts. Determining how the compressibility of hydrous mantle melts changes with pressure is of fundamental importance and is an experimental priority. Does compressibility decrease more rapidly with pressure than in anhydrous melts? Or are the pressure derivatives of the bulk moduli (K') in hydrous and anhydrous liquids

comparable? New work (Matsukage et al., 2005; Sakamaki et al., 2006) using the sink/float technique (Agee and Walker, 1988b) in the multi-anvil device on hydrous iron-rich peridotite melt and hydrous mid-ocean ridge basalt have given the first glimpse of compressibility at mantle conditions. However more experiments are needed to establish equations of state and answer the fundamental questions about role of hydrous magmas in planetary differentiation. In order to further our knowledge in this area, we present here new data on the compressibility and high pressure density of iron-rich komatiite melt with 2 and 5 wt.% dissolved water.

## 2. Experimental technique

The sink/float method has been used with success to bracket the densities of a wide range of anhydrous silicate liquids from 0.5–20 GPa (Agee, 1998; Agee and Walker, 1993; Suzuki et al., 1995; Ohtani and Maeda, 2001; Agee and Walker, 1988b; Circone and Agee, 1996; Smith and Agee, 1997; Ohtani et al., 1995; Agee, 1992a,b; Taniguchi, 1989; Suzuki et al., 1998; Knoche and Luth, 1996). In the sink/float method the density of the liquid relative to spheres of known density is determined by the sinking (more dense) or floating (less dense) of spheres in the liquid. The advantage to this method is simplicity: experimental parameters can be measured accurately (pressure, temperature, liquid composition, did the spheres sink or float?), and liquid density is measured directly under equilibrium static compression conditions. Experimental charges consist of two spheres (300–500  $\mu\text{m}$  diameter, 1 each at the top and bottom of the capsule) packed in approximately 10 mg of the ground starting material. Experiments are brought to pressure and temperature, held for a few minutes, then quenched isobarically. The sectioned quenched run product reveals the final position of the spheres (top = float, bottom = sink) allowing the determination for whether spheres were more dense or less dense than the liquid, providing an upper or lower bracket. The uncertainty on the silicate liquid density can be less than 1% relative error and is governed primarily by the uncertainty in the EOS of the crystalline spheres, temperature, pressure, and the narrowness of the sink/float  $P$ – $T$  bracket. Normally, several experiments over small pressure increments are required to obtain a narrow density bracket.

In this study, experiments in the pressure range 1.35–1.8 GPa were performed in a 0.5" bore piston–cylinder apparatus (PCA) QUICKpress from Depths of the Earth Company. A Walker-style multi-anvil device was used

for experiments at pressures 1.9–10.0 GPa. In this set up MA cubes with a truncation-edge-length (TEL) of 8 mm were employed. Both the PCA and MA contained the identical cylindrical capsule dimensions (1.5 mm long  $\times$  1 mm diameter). Estimated uncertainties in  $P$  and  $T$  are  $\pm 0.1$  GPa,  $\pm 5$   $^{\circ}\text{C}$  (PCA) and  $\pm 0.25$  GPa,  $\pm 20$   $^{\circ}\text{C}$  (MA). All sample capsules were of thick-walled high purity Mo with a friction fit lid that becomes a cold seal weld at high pressure during the experiment. Low viscosity ultrabasic melts (Liebske et al., 2005) such as used here require only short run durations ( $\sim 30$  s) for buoyancy force to move spheres up or down in the liquid sample. Even with a density differences as low as  $0.01$   $\text{g cm}^{-3}$  between liquid and spheres, settling velocities allow sinking or floating spheres to easily traverse the  $\sim 1$  mm capsule length during the 30 s run. At density differences  $< 0.01$   $\text{g cm}^{-3}$  settling velocities approach zero, and we observed this in some experiments as “neutral buoyancy” when spheres remained stationary during the experiment. The short run time minimizes contamination of the sample and reaction of the spheres with the silicate liquid. Fig. 1 shows two examples of garnet spheres that constitute a float and sink. For further details on the sink/float method used in our laboratory see for example (Circone and Agee, 1996).

Starting materials were mechanical mixtures of natural komatiite “B-4” from Belingwe (Agee and Walker, 1988b), synthetic fayalite (Agee, 1992a), reagent grade  $\text{SiO}_2$ ,  $\text{Al}_2\text{O}_3$ , and  $\text{CaO}$  powders. Water was added to the mechanical mixture in the form of brucite ( $\text{MgOOH}$ ). The nominal liquid mixture at experimental conditions was 50 wt.% komatiite and 50 wt.% fayalite with 5 wt.% water added. Thus the ideal starting composition in weight percent was  $\text{SiO}_2=36.7$   $\text{Al}_2\text{O}_3=2.9$   $\text{FeO}=38.9$   $\text{MgO}=13.5$   $\text{CaO}=2.9$   $\text{H}_2\text{O}=5.0$ . As we discuss below, most experiments in the 1400–1500  $^{\circ}\text{C}$  range retained the 5 wt.% water in the run products. Experiments in the range 1750–1860  $^{\circ}\text{C}$  retained only  $\sim 2$  wt.% water in the run products, presumably owing to water loss during the 30 s sink/float at these highest temperatures.

Buoyancy spheres were all abraded from gem quality material using a Bond air mill (Bond, 1951). Synthetic forsterite (Fo100) and natural San Carlos olivine (Fo91-90) were appropriate for sink/float measurements at lower pressures. Garnets (Py58Alm34Gr08, Py62Alm35Gr03, Py64Alm28Gr08, Py65Alm28Gr08, Py69Alm17Gr14, Py74Alm14Gr12, Py77Alm14Gr09; Py = pyrope, Alm = almandine Gr = grossular) were appropriate for sink/float measurements at higher pressure. The sphere densities at pressure and temperature of sink/float experiments were calculated after the method of Circone

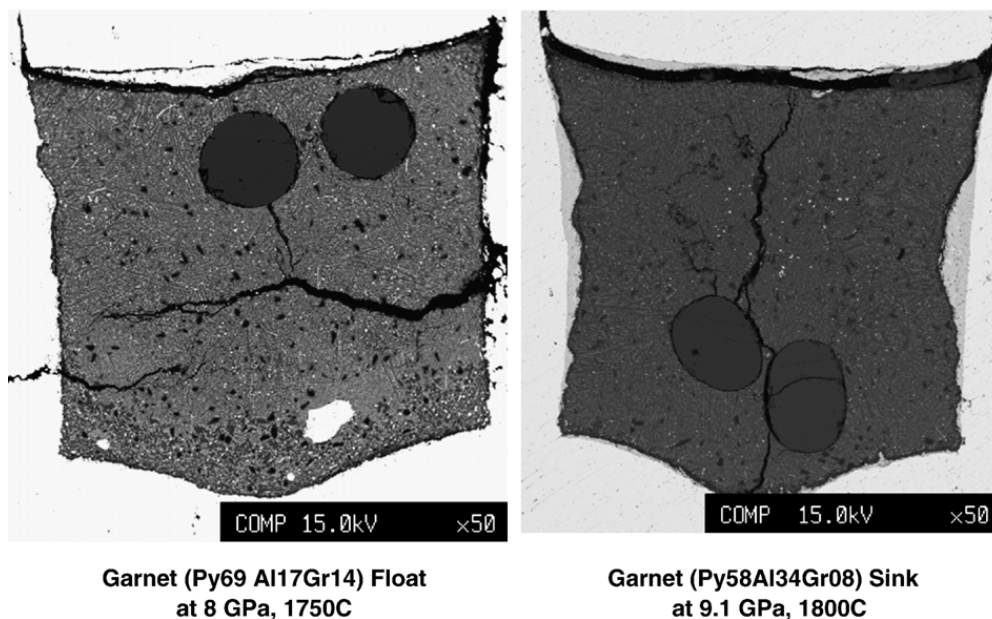
50% Komatiite + 50% Fayalite with 2wt % H<sub>2</sub>O

Fig. 1. Backscatter electron images of two sectioned run products showing typical positions of mineral marker spheres in a “float” (left) and a “sink” (right) in silicate melt. The silicate melt is now quench crystals and glass. The cracks occurred during decompression.

and Agee (1996), using the Birch–Murnaghan equation of state:

$$P = \frac{3}{2} K_T \left[ \left( \frac{\rho_{T,P}}{\rho_{T,0}} \right)^{7/3} - \left( \frac{\rho_{T,P}}{\rho_{T,0}} \right)^{5/3} \right] \left[ 1 - \frac{3}{4} (4 - K') \left( \left( \frac{\rho_{T,P}}{\rho_{T,0}} \right)^{2/3} - 1 \right) \right]$$

in which  $P$  is pressure,  $K_T$  is the isothermal bulk modulus,  $K'$  is the pressure derivative, and  $\rho_{T,0}$  and  $\rho_{T,P}$  are the densities of the sphere at temperature and at  $10^5$  Pa or high pressure.

### 3. Experimental results

Table 1 summarizes the experimental results of this study. Each experiment was sectioned and polished to reveal the position of the spheres at quench (bottom/sink or top/float?) and to confirm that the sample had been liquid during the run. Electron microprobe analyses were performed to determine the major element composition as a check on contamination of the starting material during the run. The silicate liquid in these experiments does not quench to a glass, rather it solidifies to a mass of metastable quench crystals and interstitial glass. Therefore numerous broad beam analyses were performed to determine the average value of each silicate liquid. On average 4.4 wt.% FeO was lost from the ideal starting composition of the silicate liquids, and this alloyed with the interior surface of the molybdenum capsule; and an

average of 3.6 wt.% MoO<sub>3</sub> was dissolved in the silicate liquids during the experiment.

Electron microprobe analyses were also performed on the quenched silicate liquids to confirm water retention during the experiments. This was accomplished by probing the quenched liquids for oxygen. The samples were analyzed using a JEOL 8200 electron microprobe at the Institute of Meteoritics, University of New Mexico. Analyses were conducted at 15 kV accelerating voltage, a beam current of 20 nA, and a spot size of 25  $\mu$ m. Natural mineral standards were used as calibration standards using 20 s counting times for major elements (except oxygen) and 30 s for minor elements; backgrounds were counted for 10 and 15 s, respectively. Oxygen was analyzed on a layered dispersive crystal (Ovonics Corp., Troy, MI), a synthetic crystal consisting of layers of Si and W with a 2-d spacing of 5.98 nm, specifically designed for the analysis of N, O and F. This type of crystal has been extensively tested and provides a significant count rate improvement over conventional Pb-stearate crystals. In addition, the oxygen count rate is measured using the integrated area under the peak, rather than just peak and background measurements. This method accounts for differences in peak shapes due to chemical shifts and peak shape alterations between sample and standard in order to provide more accurate measurements. Total integrated counting time for oxygen was 41 s, using an almandine mineral standard

Table 1

Run	B16-2		B16-14		B16-15		B16-16		B16-20		B16-22		B16-24			
<i>P</i> (GPa)	3.0		3.4		2.9		2.5		1.35		1.6		3.6			
<i>T</i> (°C)	1500		1500		1500		1500		1400		1400		1508			
Spheres	Fo91.2		Fo100		Fo100		Fo100		Fo100		Fo100		Fo90.3			
Result	Sink		Float		Float		Float		Sink		Sink		Sink			
# of melt analyses	13	S.D.	17	S.D.	16	S.D.	19	S.D.	18	S.D.	14	S.D.	19	S.D.		
SiO <sub>2</sub>	35.39	1.58	36.07	1.19	35.86	1.61	35.18	1.53	36.55	1.15	36.28	1.44	35.41	1.54		
TiO <sub>2</sub>	0.08	0.04	0.06	0.03	0.07	0.03	0.08	0.04	0.06	0.02	0.06	0.03	0.06	0.03		
Al <sub>2</sub> O <sub>3</sub>	3.36	1.54	3.10	1.12	3.39	1.45	4.12	1.95	4.27	1.49	4.59	1.76	2.87	1.52		
Cr <sub>2</sub> O <sub>3</sub>	0.01	0.01	0.01	0.00	0.01	0.01	0.01	0.01	0.01	0.01	0.01	0.01	0.01	0.01		
MnO	0.06	0.01	0.06	0.02	0.05	0.02	0.06	0.01	0.06	0.02	0.06	0.02	0.06	0.01		
FeO	34.14	3.48	34.52	2.29	35.54	2.96	33.82	3.28	33.49	2.21	34.69	3.12	34.42	2.52		
MgO	14.47	4.25	15.10	3.14	13.36	3.37	12.58	4.56	14.35	3.53	13.76	3.35	16.13	3.97		
CaO	2.61	1.43	2.39	0.91	2.66	1.22	3.03	1.61	2.78	1.05	2.68	1.13	2.18	1.15		
Na <sub>2</sub> O	0.07	0.04	0.10	0.05	0.14	0.08	0.12	0.07	0.08	0.04	0.09	0.04	0.07	0.05		
MoO <sub>3</sub>	3.79	1.70	3.03	1.06	3.09	1.56	4.46	1.71	2.86	1.31	2.37	1.23	3.77	1.34		
H <sub>2</sub> O	4.72	2.25	5.53	1.18	5.40	1.85	6.02	2.24	5.58	0.69	5.30	1.13	4.90	1.33		
Total (wt.%)	98.7	0.92	99.96	0.77	99.57	0.67	99.48	0.81	100.08	0.81	99.91	0.81	99.87	0.80		
$\rho$ sphere at <i>P</i> , <i>T</i> (g/cc)	3.24		3.15		3.13		3.12		3.10		3.11		3.27			
$\rho$ liquid at <i>P</i> , <i>T</i> (g/cc)	<3.24		>3.15		>3.13		>3.12		<3.10		<3.11		<3.27			
$\rho$ liquid at <i>P</i> , 1500norm	3.24		3.14		3.13		3.12		3.07		3.08		3.27			
Run	B16-7		B16-8		B16-9		B16-10		B16-11		B16-12		B16-13			
<i>P</i> (GPa)	8.1		7.9		8.6		9.1		10.0		7.5		7.9			
<i>T</i> (°C)	1750		1765		1780		1800		1860		1750		1750			
Spheres	Py62		Py65		Py64		Py58		Py58		Py74		Py77			
Result	Sink		Sink		Sink		Sink		Sink		NB		Float			
# of melt analyses	19	S.D.	20	S.D.	19	S.D.	18	S.D.	19	S.D.	17	S.D.	16	S.D.		
SiO <sub>2</sub>	39.82	3.25	39.77	2.03	39.06	2.31	41.39	2.78	39.42	2.63	37.68	1.97	42.39	3.92		
TiO <sub>2</sub>	0.07	0.03	0.08	0.02	0.08	0.02	0.06	0.02	0.08	0.02	0.08	0.02	0.07	0.03		
Al <sub>2</sub> O <sub>3</sub>	1.77	0.89	2.26	0.84	1.69	0.55	1.33	0.37	1.93	0.64	2.05	0.80	2.44	0.96		
Cr <sub>2</sub> O <sub>3</sub>	0.01	0.01	0.01	0.01	0.01	0.01	0.01	0.01	0.02	0.01	0.01	0.01	0.01	0.01		
MnO	0.06	0.01	0.07	0.02	0.06	0.02	0.06	0.02	0.06	0.02	0.06	0.02	0.07	0.02		
FeO	35.15	3.90	35.33	2.19	35.33	3.14	33.47	3.07	34.39	3.11	35.61	2.88	29.96	4.75		
MgO	14.15	1.83	14.36	1.26	13.74	1.23	14.65	1.39	14.31	1.24	13.53	1.26	15.76	2.90		
CaO	3.27	0.46	3.28	0.18	3.48	0.41	3.54	0.38	3.35	0.19	3.11	0.27	3.30	0.70		
Na <sub>2</sub> O	0.07	0.03	0.08	0.02	0.08	0.02	0.09	0.02	0.17	0.03	0.07	0.02	0.09	0.02		
MoO <sub>3</sub>	3.30	1.86	2.66	1.76	5.27	1.17	2.87	1.87	4.07	1.58	5.80	1.36	3.96	1.34		
H <sub>2</sub> O	2.23	0.62	2.30	0.65	1.83	0.56	2.13	0.44	2.17	0.68	1.73	0.97	1.26	1.26		
Total (wt.%)	99.92	0.59	100.18	0.53	100.66	0.74	99.61	0.54	99.97	0.98	99.74	0.88	99.31	0.95		
$\rho$ sphere at <i>P</i> , <i>T</i> (g/cc)	3.79		3.73		3.74		3.79		3.81		3.65		3.63			
$\rho$ liquid at <i>P</i> , <i>T</i> (g/cc)	<3.79		<3.73		<3.74		<3.79		<3.81		3.65		>3.63			
$\rho$ liquid at <i>P</i> , 1800norm	3.77		3.72		3.74		3.79		3.83		3.63		3.61			
Run	B16-3		B16-17		B16-21		B16-6		A-6-1		A-6-2		A-6-3		A-6-4	
<i>P</i> (GPa)	4.0		1.9		1.8		8.0		1.0		1.0		1.2		1.4	
<i>T</i> (°C)	1490		1490		1445		1750		1400		1425		1450		1460	
Spheres	Fo90.6		Fo100		Fo100		Py69		Fo91		Fo91		Fo91		Fo91	
Result	NB		Float		Float		Float		Sink		Sink		Float		Float	
# of melt analyses	9	S.D.	16	S.D.	36	S.D.	7	S.D.								
SiO <sub>2</sub>	36.87	5.16	34.90	1.09	34.10	1.47	37.58	2.20								
TiO <sub>2</sub>	0.04	0.03	0.07	0.03	0.04	0.03	0.08	0.03								
Al <sub>2</sub> O <sub>3</sub>	3.03	2.69	4.02	1.76	2.08	1.34	1.63	0.56								
Cr <sub>2</sub> O <sub>3</sub>	0.02	0.02	0.01	0.01	0.01	0.01	0.01	0.01								
MnO	0.06	0.02	0.05	0.01	0.05	0.02	0.06	0.02								
FeO	33.82	7.58	34.93	1.93	36.27	2.52	35.90	2.66								
MgO	19.87	7.33	14.72	3.53	18.07	4.72	13.55	1.27								
CaO	1.36	1.05	2.40	1.01	1.61	0.98	3.14	0.33								

(continued on next page)

Table 1 (continued)

Run	B16-3		B16-17		B16-21		B16-6		A-6-1	A-6-2	A-6-3	A-6-4
# of melt analyses	9	S.D.	16	S.D.	36	S.D.	7	S.D.				
Na <sub>2</sub> O	0.03	0.03	0.07	0.04	0.05	0.04	0.07	0.02				
MoO <sub>3</sub>	0.98	0.95	3.52	1.03	3.03	2.10	5.61	2.00				
H <sub>2</sub> O	2.73	1.08	3.59	1.07	3.88	1.25	0.54	0.56				
Total (wt.%)	98.81	0.84	98.29	0.73	99.19	1.07	98.16	0.56	98.71	97.11	97.74	97.13
$\rho$ sphere at $T$ (g/cc)	3.28		3.11		3.11		3.69		3.24	3.24	3.23	3.25
$\rho$ liquid at, $T$ (g/cc)	>3.28		>3.11		<3.11		>3.69		<3.24	<3.24	>3.23	>3.25

(Mcguire et al., 1992). A Phi–Rho–Z program supplied with the JEOL software was used to reduce the raw data to elemental weight percent. Water was determined from the measured oxygen by first assigning the appropriate number of moles of oxygen to measured cations, summing the results, and calculating H<sub>2</sub>O from the remaining oxygen. A kaersutite mineral standard with 1.64 wt.% H<sub>2</sub>O (Mcguire et al., 1992) was measured several times during each analytical run to monitor the quality of the analysis and relative error. The error for oxygen measured with this method was around 3% relative, and the error for H<sub>2</sub>O was less than 5% relative.

The direct determination of oxygen can provide a reliable indirect estimate of the water content of the sample (Nash, 1992). This method works particularly well and recovers SIMS and manometric water analyses when the valence states of the major cations of the sample are well known. Our experiments were run at relatively low oxygen fugacity governed by the Fe–FeO

and Mo–MoO<sub>3</sub> exchanges between sample and capsule, thus we expect to have negligible Fe<sup>+3</sup> in the silicate liquid and no excess oxygen associated with it. The silicate liquid starting composition has only trace amounts of Na<sup>+</sup>, therefore none of the excess oxygen can be attributed to volatility of sodium under the electron beam.

The sink/float experiments in this study fall into two main categories, 1) those that retained all the initial 5 wt.% H<sub>2</sub>O after quenching (top row in Table 1,  $T=1400$ – $1508$  °C,  $P=1.35$ – $3.6$  GPa), and 2) those that retained only 2 wt.% H<sub>2</sub>O after quenching (second row in Table 1,  $T=1750$ – $1860$  °C,  $P=7.5$ – $10.0$  GPa). It is assumed that water was lost from the second group of experiments and not from the first group because of higher temperatures of the second group. The data in this study are therefore presented as two separate komatiite–fayalite compositions, one with 5 wt.% H<sub>2</sub>O and one with 2 wt.% H<sub>2</sub>O. Row 3 of Table 1 also gives analyses of four experiments

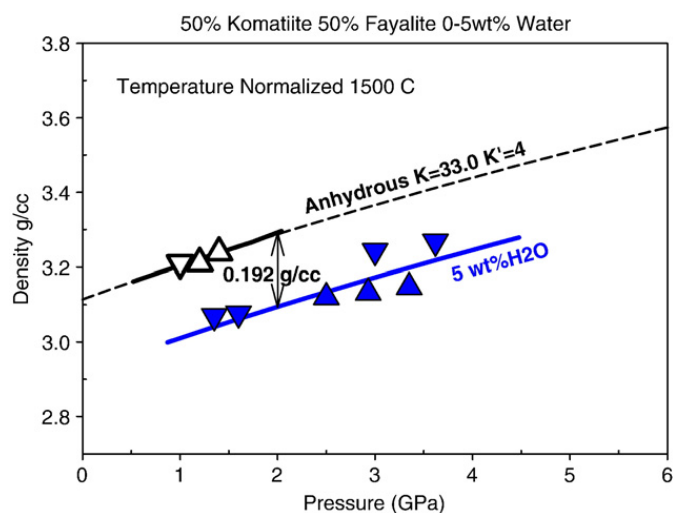


Fig. 2. Density versus pressure diagram showing olivine sinks (triangles down) and olivine floats (triangles up) for anhydrous 50–50 liquid mixture of fayalite and komatiite (open triangles) and 50–50 liquid mixture of fayalite and komatiite with 5 wt.% water added (filled triangles). Solid lines are best-fit third-order Birch–Murnaghan (BM3) curves, assuming  $K'=4$ , indicating the pressure range where the density of the silicate liquid is well constrained by the sinks and floats. Within the pressure interval of the sink and float experiments, the isothermal bulk modulus ( $K_T$ ) is similar for the hydrous liquid (30.5 GPa) and the anhydrous liquid (33.0 GPa). Dashed lines are extrapolations to higher and lower pressures where density values are less certain. The sink/float data have been normalized to 1500 °C by applying a thermal expansion correction (see Table 1).

that retained 2.7, 3.6, 3.9, and 0.5 wt.% H<sub>2</sub>O which fall outside the two main groups and were not included in the discussion below. Row 3 also has data for four anhydrous experiments of the komatiite–fayalite 50–50 mixture from Agee and Walker (1988b) that are used for comparison purposes.

### 3.1. Compressibility of komatiite–fayalite liquid with 5 wt.% water

Fig. 2 presents the observed four sinks and three floats of olivines in the group of experiments that retained, based on oxygen microprobe analyses, the initial 5 wt.% water of the komatiite–fayalite starting composition. The average calculated H<sub>2</sub>O content of these experiments was 5.4 wt.% H<sub>2</sub>O, with a standard deviation of 1.5 wt.%. The relatively large standard deviation comes from the heterogeneous nature of the quench melt. The sink and float data symbols are the calculated densities of the olivines at  $P$  and  $T$ , and they bracket the pressure–density coordinates of the hydrous silicate liquid tightly at several  $P$ – $\rho$  coordinates, for example at 2.05 GPa and 3.098 g cm<sup>-3</sup> and 3.48 GPa and 3.208 g cm<sup>-3</sup>. The bracketed densities were fit to the third order Birch–Murnaghan equation (BM3) that is shown as the 5 wt.% curve in Fig. 2. The isothermal bulk modulus ( $K_T$ ) for this curve is 30.5 GPa, assuming that the pressure derivative of the bulk modulus ( $K'$ ) is 4. For comparison, Fig. 2 also shows sink/float density brackets for anhydrous komatiite–fayalite liquid from an earlier study (Agee and Walker, 1988b). At 2 GPa the

hydrous silicate liquid is approximately 0.192 g cm<sup>-3</sup> less dense than the anhydrous silicate liquid. This gives a partial molar volume of H<sub>2</sub>O in komatiite–fayalite liquid ( $\bar{V}_{\text{H}_2\text{O}}$ ) at 1500 °C and 2 GPa of  $\sim 7$  cm<sup>3</sup> mol<sup>-1</sup> by difference from anhydrous, which is similar to  $\bar{V}_{\text{H}_2\text{O}} = 7.5$ – $8.5$  cm<sup>3</sup> mol<sup>-1</sup> in MORB calculated for 20.0 and 16.8 GPa and 2200 °C respectively (Sakamaki et al., 2006), and  $\sim 8$  cm<sup>3</sup> mol<sup>-1</sup> in Fe-rich ultrabasic silicate liquid at 14 GPa and 1900 °C (Matsukage et al., 2005). For direct comparison with these earlier studies at higher pressure and higher temperature, the pressure and temperature derivatives of  $\bar{V}_{\text{H}_2\text{O}}$  ( $d\bar{V}_{\text{H}_2\text{O}}/dP$  and  $d\bar{V}_{\text{H}_2\text{O}}/dT$ ) are required, but are at this time not well known. One possibility is that  $d\bar{V}_{\text{H}_2\text{O}}/dP$  becomes very small at pressures of 2 GPa and above, which would explain the apparent nearly constant value of  $\bar{V}_{\text{H}_2\text{O}}$  at 2, 14, 16.8 and 20.0 GPa from three different high pressure studies.

The choice of  $K' = 4$  produces a hydrous compression curve that is approximately parallel to the anhydrous curve. If true, then this would mean that hydrous komatiite–fayalite liquid has a similar compressibility to anhydrous komatiite–fayalite at the conditions of this study. The current measurements give very firm constraints on the density of hydrous komatiite–fayalite liquid in the pressure range 1–4 GPa, indicated by the solid BM3 best-fit family of curves (solid lines) in Fig. 2. Even though the density is well constrained in this pressure interval, there are still wide range values for  $K_T$  and  $K'$  that are allowed by the data. Fig. 3 shows that some smaller values of  $K_T$  paired with larger values of  $K'$

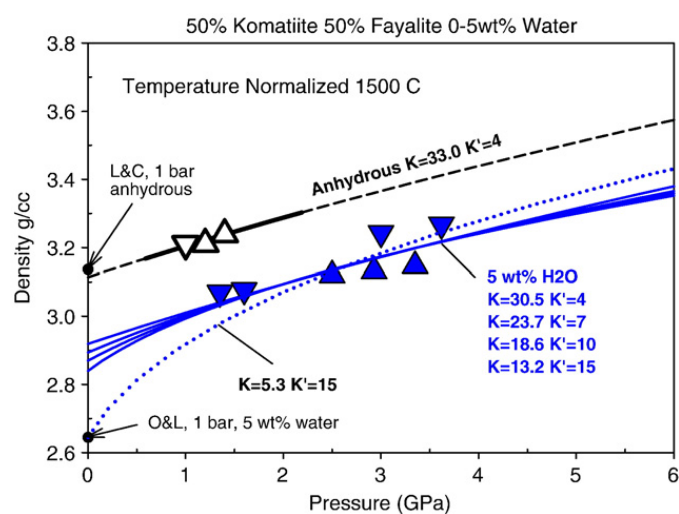


Fig. 3. Density versus pressure diagram illustrating a number of possible compression curves that satisfy the sink/float brackets of the silicate liquid with 5 wt.% water. Extrapolation of the anhydrous compression curve recovers the Lange and Carmichael (1987) calculated liquid density at 1-bar. The calculated 1-bar density of the hydrous silicate liquid using the partial molar volume of water from Ochs and Lange (1999) is in agreement with the high pressure sink/float brackets if  $K_T$  is very small and  $K'$  is large. For example, the dotted line is a compression curve with  $K_T = 5.3$  GPa and  $K' = 15$ .

also give best-fits for the sink/float brackets. If one of these fits is the correct one, then it would mean that the compressibility of hydrous komatiite–fayalite is greater than anhydrous komatiite–fayalite at lower pressure (<1 GPa), but becomes similar in compressibility at >1 GPa. This can be interpreted as a non-linear  $d\bar{V}_{\text{H}_2\text{O}}/dP$  that is large at 1-bar, decreases significantly by 1 GPa, and approaches zero at 2 GPa and above.

In previous studies on static compression of anhydrous silicate liquids, calculated 1-bar reference densities (Lange and Carmichael, 1987) were commonly combined with the high pressure data to provide a low pressure anchor for liquid compression curves. This practice was justified because of the extensive database of partial molar volumes of liquid oxides applicable to anhydrous basic and ultrabasic silicate liquids, done by direct measurements of silicate liquids using the Archimedean double-bob method. Unfortunately, the database for 1-bar molar volumes of hydrous silicate liquids, and the partial molar volume of  $\text{H}_2\text{O}$  ( $\bar{V}_{\text{H}_2\text{O}}$ ) in silicate liquids is much less complete. As mentioned above, Ochs and Lange (1999) have done 1-bar density measurements on hydrous silicate glasses which were synthesized at 1 GPa in a piston–cylinder device. They derived a value for  $\bar{V}_{\text{H}_2\text{O}}$  and a linear  $d\bar{V}_{\text{H}_2\text{O}}/dT$  in silicate liquid at 1000 °C. Recent studies on static compression of hydrous silicate liquids (Matsukage et al., 2005; Sakamaki et al., 2006) have adopted the O&L 1-bar  $\bar{V}_{\text{H}_2\text{O}}$  and  $d\bar{V}_{\text{H}_2\text{O}}/dT$  for silicate liquid to anchor their high pressure data on ultrabasic and basaltic

compositions at temperatures as much as 1200° higher than the O&L reference temperature. Future work may confirm if this approach is justified, however, O&L also studied a fairly restricted compositional range that included albite, rhyolite, and KCS glasses, (all silica-rich and iron-free). Therefore it is not clear if their derived value of  $\bar{V}_{\text{H}_2\text{O}}$  or  $d\bar{V}_{\text{H}_2\text{O}}/dT$  can be extrapolated to silica-poor, iron-rich compositions such as the komatiite–fayalite liquid of the current study or the Fe-rich compositions of Matsukage et al. (2005). On the other hand, Fig. 3 shows that the O&L 1-bar calculated density is consistent with our high pressure sink/float brackets if  $K_T$  is very small and  $K'$  is very large. For example, a BM3 compression curve with  $K_T=5.3$  GPa and  $K'=15$  anchored at the O&L 1-bar reference density passes within the sink/float bounds. However, the O&L 1-bar density is much lower than the family of best-fit curve extrapolations (solid curves in Fig. 3) and would require a very strong change in density for hydrous komatiite–fayalite liquid in the pressure range 0–1.5 GPa, suggesting an extremely non-linear  $d\bar{V}_{\text{H}_2\text{O}}/dP$ . In contrast, the extrapolated best-fit BM3 curve for anhydrous komatiite–fayalite liquid very nearly recovers the Lange and Carmichael (1987) calculated 1-bar density.

Matsukage et al. (2005) performed static compression sink/float experiments using diamonds on two silicate liquids with 5 wt.%  $\text{H}_2\text{O}$  that are similar in composition to the hydrous komatiite–fayalite composition of the current study (s5-a:  $\text{SiO}_2=33.9$   $\text{Al}_2\text{O}_3=1.6$   $\text{FeO}=24.9$   $\text{MgO}=23.6$   $\text{CaO}=11.1$   $\text{H}_2\text{O}=5.0$ ; and s6-a:

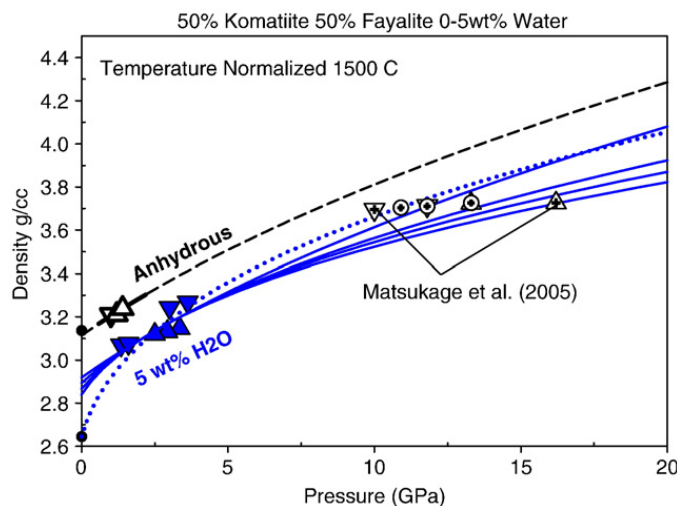


Fig. 4. Density versus pressure diagram comparing the present study with the sink/float experiments of Matsukage et al. (2005). The open symbols with crosses are sinks (triangles down), floats (triangles up), and neutral buoyancies (circles) that were done with diamond marker buoys in two iron-rich silicate liquids with 5 wt.% water that are very similar to the 50–50 komatiite–fayalite liquid mixture of this study. The bracketed densities of Matsukage et al. are in good agreement with the extrapolated BM3 curves from this study, however their relatively wide brackets do not help narrow the range of  $K$  and  $K'$  possibilities for hydrous silicate melt. The data of Matsukage et al. have been normalized to 1500 °C and to the komatiite/fayalite 50–50 mix composition.

SiO<sub>2</sub>=33.5 Al<sub>2</sub>O<sub>3</sub>=3.1 FeO=25.5 MgO=22.5 CaO=10.5 H<sub>2</sub>O=5.0). These compositions were run at 1900 °C and 10–16 GPa in rhenium capsules, and here we apply a temperature and compositional normalization to them to compare with the current data set in Fig. 4. The Matsukage sink/float brackets are consistent with the extrapolated best-fit family of BM3 curves from our experiments and also with the BM3 curve anchored by the O&L 1-bar density. Unfortunately, the Matsukage sink/float brackets are comparatively wide so they provide no guide for choosing one curve over the other as most likely for hydrous komatiite–fayalite liquid at high pressure. Matsukage et al. adopted the O&L 1-bar density for calculation of their compression curve and values for  $K_T$  and  $K'$  to fit to their high pressure sink/float data. Fig. 4 shows their compression curve (solid curve) and data for composition “s6-a”, normalized to komatiite–fayalite, and 1500 °C. Also shown in Fig. 4 is the compression curve (dashed curve) for the anhydrous komatiite–fayalite composition. The two curves, when extrapolated, intersect at ~21 GPa which is equivalent to  $\bar{V}_{\text{H}_2\text{O}}=0$ ; at higher pressures the hydrous liquid becomes denser than the anhydrous, which is equivalent to  $\bar{V}_{\text{H}_2\text{O}}<0$ . Although it cannot be completely ruled out, it seems unlikely that  $\bar{V}_{\text{H}_2\text{O}}$  becomes negative at high pressure, instead it may be more likely that the calculated compression curve for s6-a is too steep. The curve for s6-a could be less steep if the adopted value of  $K'$  were

larger, or if the adopted 1-bar reference density were higher (Fig. 5).

### 3.2. Compressibility of komatiite–fayalite liquid with 2 wt.% water

Fig. 6 presents the observed five sinks, one float, and one neutral buoyancy of garnets in the group of experiments that retained, based on oxygen microprobe analyses, 2 wt.% water of the komatiite–fayalite starting composition. The average value of these experiments was 2.0 wt.% H<sub>2</sub>O with standard deviation of 0.7 wt.%. The sink, float, and neutral data symbols are the calculated densities of the garnets at  $P$  and  $T$ . A sink and a float tightly bracket this silicate liquid at 7.9 GPa and 3.665 g cm<sup>-3</sup>. The neutral buoyancy observation also provides pressure–density coordinates for this liquid at 7.5 GPa and 3.663 g cm<sup>-3</sup>. The anhydrous liquid curve is not as well constrained as in the comparison in Section 3.1 since it is extrapolated from lower pressures and lower temperatures, thus the derived  $\bar{V}_{\text{H}_2\text{O}} \sim 4$  cm<sup>3</sup> mol<sup>-1</sup> by difference at 7.9 GPa and 1800 °C should be considered preliminary. Because the density of the 2 wt.% hydrous liquid was only determined over a narrow pressure range, no unique “best-fit” BM3 values for  $K_T$  and  $K'$  can be calculated. On the other hand, we can consider some possible compression curves that are consistent with the

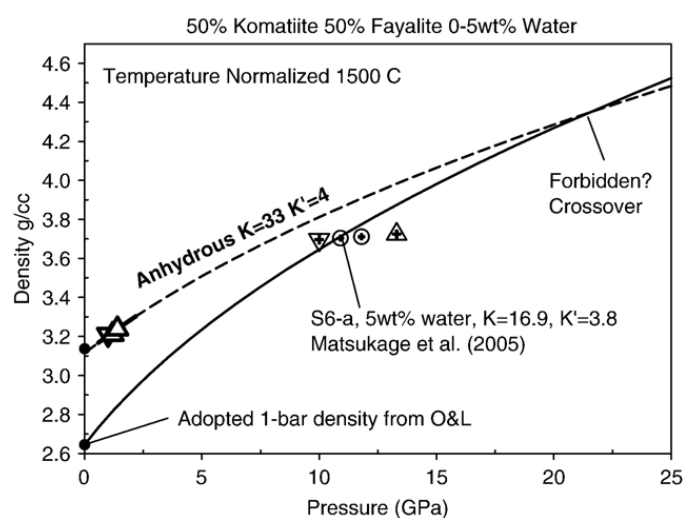


Fig. 5. Density versus pressure diagram showing an apparent “forbidden” density crossover between anhydrous komatiite/fayalite silicate melt assuming  $K_T=33$  GPa and  $K'=4$  from this study, and the same composition with 5 wt.% water with elastic constants  $K_T=16.9$  GPa and  $K'=3.8$  from Matsukage et al., (2005). The Matsukage compression curve is derived by using their sink/float density brackets at high pressure and the density of partial molar volume of water at 1-bar from Ochs and Lange (1999) combined with silicate melt density at 1-bar from Lange and Carmichael (1987). It appears that the adopted elastic constants for anhydrous and hydrous silicate melts are incompatible since they produce a density crossover with hydrous silicate melt becoming denser than anhydrous silicate melt. This crossover seems unlikely since it would require the partial molar volume of water to become negative in silicate liquid at high pressure. A density crossover is avoidable if  $K_T$  and  $K'$  of both liquids is similar or if the hydrous silicate liquid has a small  $K_T$  and large  $K'$ .

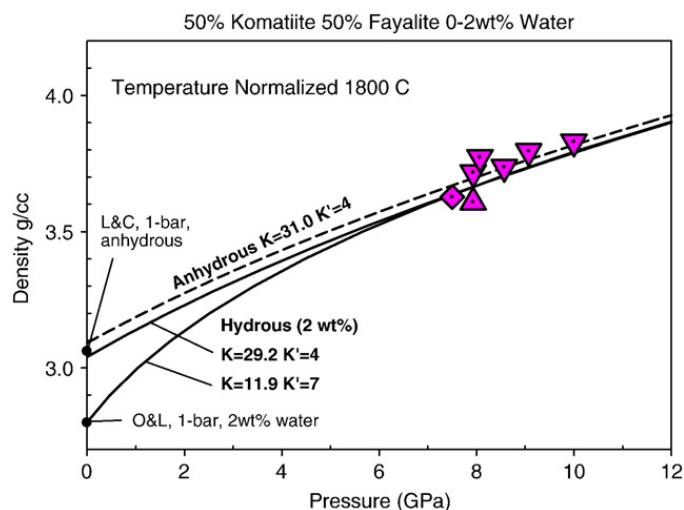


Fig. 6. Density versus pressure diagram showing garnet sinks (triangles down) and garnet floats (triangles up) for a 50–50 liquid mixture of fayalite and komatiite with 2 wt.% water. Solid lines are best-fit third-order Birch–Murnaghan (BM3) curves to the high pressure sink/float density brackets with different assumptions. The upper solid curve assumes  $K'=4$ , which gives a value of  $K_T=29.2$  GPa and is approximately parallel to the dashed curve for anhydrous komatiite/fayalite. The lower solid curve assumes a 1-bar partial molar volume for water in silicate liquid from Ochs and Lange (1999), gives values of  $K_T=11.9$  GPa and  $K'=7$ , and is much steeper in slope than the anhydrous curve in the range 0–3 GPa.

data. One possibility is that the 2 wt.% hydrous compression curve is approximately parallel to the anhydrous curve (dashed) in which case  $K_T=29.2$  GPa with  $K'=4$ . Another possibility is that the data can be anchored by the O&L 1-bar density calculation, which case  $K_T=11.9$  GPa  $K'=7$ , and assuming that the hydrous curve cannot intersect or cross over the anhydrous dashed curve. In any case, both possible curves become very similar at 6.5 GPa and above, thus they give very similar extrapolations at higher pressure, even

though they have very different low pressure (<2 GPa) trajectories down to 1-bar. Future work with additional sink/float measurements at multiple pressures will help narrow the range of possible values of  $K_T$  and  $K'$  for this composition.

#### 4. Density crossovers with equilibrium liquidus olivine

Assuming that the Fe–Mg olivine–liquid exchange coefficient  $K_D$  (Roeder and Emslie, 1970) is equal to 0.35

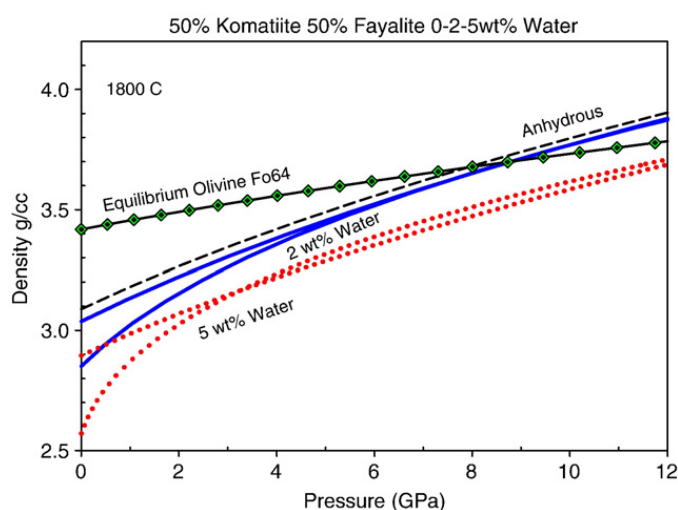


Fig. 7. Density versus pressure diagram showing the compression curve of equilibrium liquidus olivine (Fo64) compared to the compression curves of 50–50 liquid mixtures of komatiite/fayalite with 0 wt.%, 2 wt.% and 5 wt.% water normalized to 1800 °C. A density crossover exists between the anhydrous silicate liquid (dashed curve) and olivine at about 7.5 GPa. A density crossover exists between the hydrous silicate liquid with 2 wt.% water (solid curves) and olivine at about 9 GPa. No density crossover exists between olivine and the hydrous silicate liquid with 5 wt.% water (dotted curves).

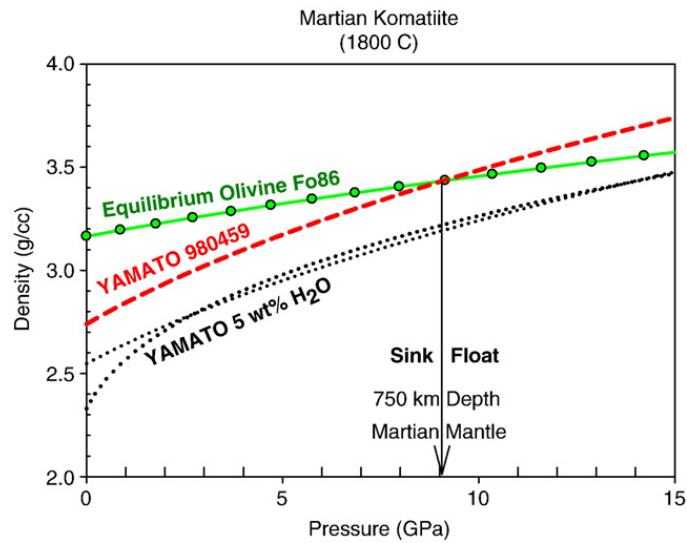


Fig. 8. Density versus pressure diagram showing the compression curve of anhydrous martian komatiite (Yamato 980459)  $K_T=25$  GPa,  $K'=4.2$  (dashed curve), possible compression curves for martian komatiite with 5 wt.% H<sub>2</sub>O  $K_T=25$  GPa,  $K'=4.2$  and  $K_T=6$  GPa,  $K'=12$  (dotted curves), and equilibrium liquidus olivine (Fo86).

we calculate that the liquidus olivine for hydrous komatiite–fayalite liquid is Fo64. In Fig. 7 the compression curve for olivine Fo64 at 1800 °C is plotted along with several possible compression curves for komatiite–fayalite with 0, 2, and 5 wt.% H<sub>2</sub>O. We see that the anhydrous liquid has a density crossover with liquidus olivine at about 8 GPa, which is consistent with previous studies of other anhydrous compositions (Agee and Walker, 1993; Suzuki et al., 1995; Agee and Walker, 1988b; Ohtani et al., 1995). The 2 wt.% H<sub>2</sub>O liquid has a density crossover with

liquidus olivine at slightly higher pressure near 9 GPa. If  $K_D$  is smaller, for instance 0.3, then the liquidus olivine will be more forsteritic and the density crossover will be a slightly lower pressures. In contrast, none of the possible compression curves (two shown for illustrative purposes) for komatiite–fayalite liquid with 5 wt.% H<sub>2</sub>O have density crossovers with equilibrium liquidus olivine. Thus there appears to be a water content value between 2 and 5 wt.% where olivine flotation in hydrous FeO-rich mantle melt becomes impossible.

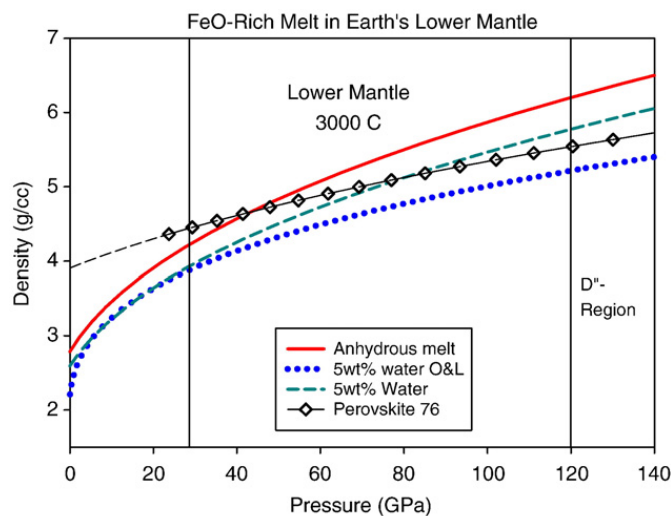


Fig. 9. Density versus pressure diagram showing the compression curve of anhydrous FeO-rich melt  $K_T=30$  GPa,  $K'=4$  (solid curve), possible compression curves for hydrous FeO-rich melt with 5 wt.% H<sub>2</sub>O  $K_T=30$  GPa,  $K'=4$  (dashed curve) and  $K_T=4.2$  GPa,  $K'=12$  (dotted curve), and equilibrium liquidus perovskite (En76).

## 5. The effect of water on planetary differentiation

Buoyancy relations between crystals and melts in hydrous Fe-rich compositions such as the one studied here are highly relevant to partial melting processes during planetary differentiation. For example, it has been widely accepted for some time that Mars accreted as a volatile-rich planet (Dreibus and Wänke, 1985). Isotopic and trace element studies of Mars meteorites indicate that the martian mantle underwent wholesale differentiation very early in its history, possibly through the solidification of deep magma ocean (Borg and Draper, 2003). If so, then the compressibility of hydrous FeO-rich silicate liquid is important for understanding buoyancy relations and whether crystals or melts sink or float in a volatile-rich magma ocean with a few percent H<sub>2</sub>O. Fig. 8 shows crystal–liquid density relations for a primitive martian melt derived from the major element composition of Mars meteorite Yamato 980459, a komatiitic shergottite with elastic constants assumed to be similar to terrestrial komatiite (Agee and Walker, 1993). This komatiite may be representative of magmas produced by melting in the martian mantle (McKay et al., 2004) or the liquid composition of an early martian magma ocean. We calculate an equilibrium liquidus olivine for this magma to be Fo86 and its anhydrous compression curve is shown in Fig. 8. The depth of the olivine/komatiite density crossover in the martian mantle would be at approximately 750 km or 9 GPa of pressure. Fig. 8 also shows two possible compression curves for martian komatiite with 5 wt.% H<sub>2</sub>O, with elastic constants consistent with a  $-0.192 \text{ g cm}^{-3}$  density difference from anhydrous at 2 GPa. Just as with komatiite–fayalite in Fig. 7, there is no density crossover between equilibrium liquidus olivine and the 5 wt. H<sub>2</sub>O Yamato liquid, thus a high water content would sink olivines at 750 km depth and below, instead of floating, and a density crossover cut-off would exist between 2 and 5 wt.% H<sub>2</sub>O content as in Fig. 7.

Our results, as applied to the Earth, are in agreement with the upper mantle transition zone being able to support a gravitationally stable hydrous melt layer atop the 410 km discontinuity (Bercovici and Karato, 2003; Ohtani et al., 2004), especially if it is an FeO-rich partial melt. FeO-rich partial melts may also reside at the base of the lower mantle in the D''-layer. Fig. 9 shows possible extrapolations of compression curves for an FeO-rich melt in the Earth's lower mantle. The anhydrous melt has a density crossover with crystalline perovskite with composition En76Fs24 at approximately 45 GPa. This perovskite maybe representative of the liquidus phase at the base of the mantle, although

other possibilities include magnesiowuestite and post-perovskite phase. FeO-rich melt with 1–2 wt.% H<sub>2</sub>O is likely to have a density crossover with perovskite in the lower mantle, however it is still unclear if FeO-rich melt with 5 wt.% H<sub>2</sub>O will float perovskite at any pressure in the Earth. For example, Fig. 9 shows two compression curves for komatiite–fayalite liquid with 5 wt.% H<sub>2</sub>O, with elastic constants consistent with a  $-0.192 \text{ g cm}^{-3}$  density difference from anhydrous at 2 GPa. One of the curves is roughly parallel to the anhydrous curve and has a density crossover with perovskite at approximately 80 GPa. The other curve begins with a very steep trajectory and is anchored at 1-bar by the calculated density from O&L, but it changes slope with pressure rapidly and diverges significantly from the anhydrous compression curve. In this case there is no density crossover with perovskite at lower mantle pressures (<140 GPa). These extrapolated third order Birch–Murnaghan compression curves highlight the uncertainty in our understanding of hydrous melts in the lower mantle. Clearly, new data at much higher pressures are needed to place firmer constraints on whether crystal–liquid density crossovers exist in the D''-layer (Lay et al., 2004) and contribute to the ultra-low seismic velocity anomalies there.

## Acknowledgements

We thank Michael Spilde for performing electron microprobe analyses and David Draper for assistance in the high pressure laboratory, and Linda Elkins-Tanton for useful comments and suggestions. This work was funded by NSF grant EAR-0509902 and NASA Grant NNG04GH1G.

## References

- Agee, C.B., 1992a. Isothermal compression of molten Fe<sub>2</sub>SiO<sub>4</sub>. *Geophys. Res. Lett.* 19, 1169–1172.
- Agee, C.B., 1992b. Thermal expansion of molten Fe<sub>2</sub>SiO<sub>4</sub> at high pressure. *Geophys. Res. Lett.* 19, 1173–1176.
- Agee, C.B., 1998. Crystal–liquid density inversions in terrestrial and lunar magmas. *Phys. Earth Planet. Inter.* 107, 63–74.
- Agee, C.B., Walker, D., 1988a. Mass balance and phase density constraints on early differentiation of chondritic mantle. *Earth Planet. Sci. Lett.* 90, 144–156.
- Agee, C.B., Walker, D., 1988b. Static compression and olivine flotation in ultrabasic silicate liquid. *J. Geophys. Res.* 93, 3437–3449.
- Agee, C.B., Walker, D., 1993. Olivine flotation in mantle melt. *Earth Planet. Sci. Lett.* 114, 315–324.
- Abe, Y., Ohtani, E., Okuchi, T., Righter, K., Drake, M.J., 2000. Water in the early Earth. In: Canup, R.M., Righter, K. (Eds.), *Origin of the Earth and Moon*. University of Arizona Press/Lunar and Planetary Institute, Tucson/Houston, pp. 413–433.

- Bercovici, D., Karato, S., 2003. Whole-mantle convection and the transition-zone water filter. *Nature* 425, 39–44.
- Bond, W.L., 1951. Making small spheres. *Rev. Sci. Instrum.* 22, 344–345.
- Borg, L.E., Draper, D.S., 2003. A petrogenetic model for the origin and compositional variation of the martian basaltic meteorites. *Meteorit. Planet. Sci.* 38, 1713–1731.
- Burnham, C.W., Davis, N.F., 1971. The role of H<sub>2</sub>O in silicate melts. I. *P–V–T* relations in the system NaAlSi<sub>3</sub>O<sub>8</sub>–H<sub>2</sub>O to 10 kilobars and 1000 °C. *Am. J. Sci.* 270, 54–79.
- Cameron, A.G.W., Benz, W., 1991. The origin of the Moon and the single impact hypothesis IV. *Icarus* 92, 204–216.
- Chabot, N.L., Draper, D.S., Agee, C.B., 2005. Conditions of core formation in the Earth: constraints from nickel and cobalt partitioning. *Geochim. Cosmochim. Acta* 69, 2141–2151.
- Circone, S., Agee, C.B., 1996. Compressibility of molten high-Ti mare glass; evidence for crystal–liquid density inversions in the lunar mantle. *Geochim. Cosmochim. Acta* 60, 2709–2720.
- Delano, J.W., 1990. Buoyancy-driven melt segregation in the Earth's moon. I. Numerical Results, Proc. of 20th Lunar and Planet. Sci. Conf., pp. 3–12.
- Dreibus, G., Wänke, H., 1985. Mars, a volatile-rich planet. *Hans Suess Festschrift* 20, 367–381.
- Green, D.H., 1973. Experimental melting studies on a model upper mantle composition at high pressure under water-saturated and water-undersaturated conditions. *Earth Planet. Sci. Lett.* 19, 37–53.
- Kleine, T., Munker, C., Mezger, K., Palme, H., 2002. Rapid accretion and early core formation on asteroids and the terrestrial planets from Hf–W chronometry. *Nature* 418, 952–955.
- Knoche, R., Luth, R.W., 1996. Density measurements on melts at high pressure using the sink/float method: limitations and possibilities. *Chem. Geol.* 128, 229–243.
- Lange, R.A., Carmichael, I.S.E., 1987. Densities of Na<sub>2</sub>O–K<sub>2</sub>O–CaO–MgO–FeO–Fe<sub>2</sub>O<sub>3</sub>–Al<sub>2</sub>O<sub>3</sub>–TiO<sub>2</sub>–SiO<sub>2</sub> liquids: new measurements and derived partial molar properties. *Geochim. Cosmochim. Acta* 51, 2931–2946.
- Lay, T., Garnero, E.J., Williams, Q., 2004. Partial melting in a thermochemical boundary layer at the base of the mantle. *Phys. Earth Planet. Inter.* 146, 441–467.
- Li, J., Agee, C.B., 1996. Geochemistry of mantle–core differentiation at high pressure. *Nature* 381, 686–689.
- Liebske, C., Schmickler, B., Terasaki, H., Poe, B.T., Suzuki, A., Funakoshi, K., Ando, R., Rubie, D.C., 2005. Viscosity of peridotite liquid up to 13 GPa: implications for magma ocean viscosities. *Earth Planet. Sci. Lett.* 240, 589–604.
- Matsukage, K.N., Jing, Z.C., Karato, S., 2005. Density of hydrous silicate melt at the conditions of Earth's deep upper mantle. *Nature* 438, 488–491.
- McGuire, A.V., Francis, C.A., Dyar, M.D., 1992. Mineral standards for electron-microprobe analysis of oxygen. *Am. Mineral.* 77, 1087–1091.
- McKay, G., Le, L., Schwandt, C., Mikouchi, T., Koizumi, E., Jones, J.H., 2004. Yamato 980459: the most primitive shergottite? *Lunar Planet. Sci.* XXXV, 2154.
- McSween Jr., H.Y., Grove, T.L., Lentz, R.C.F., Dann, J.C., Holzheid, A.H., Riciputi, L.R., Ryan, J.G., 2001. Geochemical evidence for magmatic water within Mars from pyroxenes in the Shergotty meteorite. *Nature* 409, 487–490.
- Miller, G.H., Stolper, E.M., Ahrens, T.J., 1991a. The equation of state of a molten komatiite, 1, shock wave compression to 36 GPa. *J. Geophys. Res.* 96, 11,831–11,848.
- Miller, G.H., Stolper, E.M., Ahrens, T.J., 1991b. The equation of state of molten komatiite, 2, application to komatiite petrogenesis and the Hadean mantle. *J. Geophys. Res.* 96, 11,849–11,864.
- Morse, S.A., 1993. Behavior of a perched crystal layer in a magma ocean. *J. Geophys. Res.* 98, 5347–5353.
- Nash, W.P., 1992. Analysis of oxygen with the electron-microprobe—applications to hydrated glass and minerals. *Am. Mineral.* 77, 453–456.
- Nisbet, E.G., Walker, D., 1982. Komatiites and the structure of the Archean mantle. *Earth Planet. Sci. Lett.* 60, 105–113.
- Nolet, G., Zielhuis, A., 1994. Low S velocities under the Tornquist–Tesseyre zone: evidence for water injection into the transition zone by subduction. *J. Geophys. Res.* 99, 15,813–15,820.
- Ochs, F.A., Lange, R.A., 1997. The partial molar volume, thermal expansivity and compressibility of H<sub>2</sub>O in NaAlSi<sub>3</sub>O<sub>8</sub> liquid: new measurements and an internally consistent model. *Contrib. Mineral. Petrol.* 129, 155–165.
- Ochs, F.A., Lange, R.A., 1999. The density of hydrous magmatic liquids. *Science* 283, 1315–1317.
- Ohtani, E., 1983. Melting temperature distribution and fractionation in the lower mantle. *Phys. Earth Planet. Inter.* 33, 12–25.
- Ohtani, E., 1984. Generation of komatiite magma and gravitational differentiation in the deep upper mantle. *Earth Planet. Sci. Lett.* 67, 261–272.
- Ohtani, E., 1985. The primordial terrestrial magma ocean and its implication for stratification of the mantle. *Phys. Earth Planet. Inter.* 38, 70–80.
- Ohtani, E., 1987. Ultrahigh pressure melting of a model chondritic mantle and pyrolite compositions. In: Manghnan, M.H., Syono, Y. (Eds.), *High-Pressure Research in Mineral Physics*. Terra/AGU, Tokyo/Washington, D.C., pp. 87–93.
- Ohtani, E., Maeda, M., 2001. Density of basaltic melt at high pressure and stability of the melt at the base of the lower mantle. *Earth Planet. Sci. Lett.* 193, 69–75.
- Ohtani, E., Nagata, Y., Suzuki, A., Kato, T., 1995. Melting relations of peridotite and the density crossover in planetary mantles. *Chem. Geol.* 120, 207–221.
- Ohtani, E., Litasov, K., Hosoya, T., Kubo, T., Kondo, T., 2004. Water transport into the deep mantle and formation of a hydrous transition zone. *Phys. Earth Planet. Inter.* 143–44, 255–269.
- Revenaugh, J., Sipkin, S.A., 1994. Seismic evidence for silicate melt atop the 410-km mantle discontinuity. *Nature* 369, 474–476.
- Rigden, S.M., Ahrens, T.J., Stolper, E.M., 1984. Densities of liquid silicates at high pressures. *Science* 226, 1071–1074.
- Rigden, S.M., Ahrens, T.J., Stolper, E.M., 1988. Shock compression of molten silicate: results for a model basaltic composition. *J. Geophys. Res.* 93, 367–382.
- Roeder, P.L., Emslie, R.F., 1970. Olivine–liquid equilibrium. *Contrib. Mineral. Petrol.* 29, 275–289.
- Sakamaki, T., Suzuki, A., Ohtani, E., 2006. Stability of hydrous melt at the base of the Earth's upper mantle. *Nature* 439, 192–194.
- Smith, J.R., Agee, C.B., 1997. Compressibility of molten “green glass” and crystal–liquid density crossovers in low-Ti lunar magma. *Geochim. Cosmochim. Acta* 61, 2139–2145.
- Solomatov, V.S., Stevenson, D.J., 1993. Suspension in convective layers and style of differentiation of a terrestrial magma ocean. *J. Geophys. Res.* 98, 5375–5390.
- Solomon, S.C., Aharonson, O., Aurnou, J.M., Banerdt, W.B., Carr, M.H., Dombard, A.J., Frey, H.V., Golombek, M.P., Hauck, S.A., Head, J.W., Jakosky, B.M., Johnson, C.L., McGovern, P.J., Neumann, G.A., Phillips, R.J., Smith, D.E., Zuber, M.T., 2005. New perspectives on ancient Mars. *Science* 307, 1214–1220.

- Stolper, E.M., Walker, D., Hager, B.H., Hays, J.F., 1981. Melt segregation from partially molten source regions: the importance of melt density and source region size. *J. Geophys. Res.* 86, 6261–6271.
- Suzuki, A., Ohtani, E., Kato, T., 1995. Flotation of diamond in mantle melt at high pressure. *Science* 269, 216–218.
- Suzuki, A., Ohtani, E., Kato, T., 1998. Density and thermal expansion of a peridotite melt at high pressure. *Phys. Earth Planet. Inter.* 107, 53–61.
- Taniguchi, H., 1989. Densities of melts in the system  $\text{CaMgSi}_2\text{O}_6$ – $\text{CaAl}_2\text{Si}_2\text{O}_8$  at low and high pressures, and their structural significance. *Contrib. Mineral. Petrol.* 103, 325–334.
- Williams, Q., Garnero, E., 1998. Seismic evidence for partial melt at the base of the Earth's mantle. *Science* 273, 1528–1530.
- Yin, Q., Jacobsen, S.B., Yamashita, K., Blichert-Toft, J., Telouk, P., Albarede, F., 2002. A short timescale for terrestrial planet formation from Hf–W chronometry of meteorites. *Nature* 418, 949–952.